$K_{10}M_4M'_4S_{17}$ (M = Mn, Fe, Co, Zn; M′ = Sn, Ge) and $Cs_{10}Cd_4Sn_4S_{17}$: Compounds with a Discrete Supertetrahedral Cluster

Oleg Palchik, Ratnasabapathy G. Iyer, Christian G. Canlas, David P. Weliky, and Mercouri G. Kanatzidis*

East Lansing, Michigan / USA, Department of Chemistry, Michigan State University

Received May 10th, 2004.

Dedicated to Professor Martin Jansen on the Occasion of his 60th Birthday

Abstract. The cluster compounds $K_{10}Zn_4Sn_4S_{17}$, $K_{10}Mn_4Sn_4S_{17}$, $K_{10}Fe_4Sn_4S_{17}$, $K_{10}Co_4Sn_4S_{17}$, $Cs_{10}Cd_4Sn_4S_{17}$ and $K_{10}Zn_4Ge_4S_{17}$ are described. The structures of these compounds, refined by single-crystal X-ray diffraction techniques, contain the discrete cluster $[M_4M'_4S_{17}]^{10-}$ (M = Zn, Mn, Co, Fe, Cd; M′ = Sn or Ge) which has the structure of $Si_8C_{17}H_{36}$. It is built from the sulfur-connected tetrahedral SnS_4 and MS_4 units with the additional quadruply bridging sulfur atom at the center of the cluster. All compound show some solubility and stability in water and formamide. $Cs_{10}Cd_4Sn_4S_{17}$ and $K_{10}Zn_4Ge_4S_{17}$ show photoluminescence at room temperature.The magnetic properties of $K_{10}Mn_4Sn_4S_{17}$, $K_{10}Fe_4Sn_4S_{17}$, $K_{10}Co_4Sn_4S_{17}$ indicate strong antiferromagnetic interactions arising from spin coupling within the cluster but their magnetic susceptibility is characterized with a discrepancy between field-cooled and zero field-cooled measurements.

Keywords: Cluster compound; Tin; Germanium; Sulfides

$K_{10}M_4M'_4S_{17}$ (M = Mn, Fe, Co, Zn; M′ = Sn, Ge) und $Cs_{10}Cd_4Sn_4S_{17}$: Verbindungen mit einem diskreten supertetraedrischen Cluster

Inhaltsübersicht. Die Cluster-Verbindungen $K_{10}Zn_4Sn_4S_{17}$, $K_{10}Mn_4Sn_4S_{17}$, $K_{10}Fe_4Sn_4S_{17}$, $K_{10}Co_4Sn_4S_{17}$, $Cs_{10}Cd_4Sn_4S_{17}$ und $K_{10}Zn_4Ge_4S_{17}$ werden beschrieben. Die Strukturen dieser Verbindungen wurden durch Einkristall-Röntgenstrukturanalyse bestimmt. Sie enthalten diskrete Cluster von $[M_4M'_4S_{17}]^{10-}$ (M = Zn, Mn, Co, Fe, Cd; M′ = Sn or Ge), die die Struktur von $Si_8C_{17}H_{36}$ haben. Sie werden aus über Schwefelatomen verbundenen tetraedrischen SnS_4- und MS_4-Einheiten aufgebaut mit dem zusätzlich vierfach verbrückenden Schwefelatom im Zentrum des Clusters. Alle Verbindungen sind etwas löslich und stabil in Wasser und Formamid. $Cs_{10}Cd_4Sn_4S_{17}$ und $K_{10}Zn_4Ge_4S_{17}$ zeigen Photolumineszens bei Zimmertemperatur. Die magnetischen Eigenschaften von $K_{10}Mn_4Sn_4S_{17}$, $K_{10}Fe_4Sn_4S_{17}$, $K_{10}Co_4Sn_4S_{17}$ zeigen starke antiferromagnetische Wechselwirkungen aufgrund der Spin-Kupplung in den Clustern, während ihre magnetischen Suszeptibilitäten durch eine Diskrepanz zwischen Kaltfeld- und Null-Kaltfeld-Messungen charakterisiert wird.

Introduction

The availability of large metal chalcogenido clusters that can be put into solution is of general chemical interest because they could serve as convenient precursors for the preparation of novel nano- or mesoporous materials [1, 2]. The use of such precursors may allow more rational synthetic approaches for a wide variety of solids with semiconducting and/or micro/mesoporous properties. Recently a group of chalcogenide cluster-based solids with large pores filled with exchangeable organic cations has emerged with novel properties and structural features [3, 4, 5]. The clusters in these materials are generally adamantine-type belonging to the T*n* homologous series where *n* is the cluster "generation" [6]. A T1 cluster is the simple tetrahedral unit $[GeS_4]^{4-}$, the T2 cluster refers to the adamantane cluster $[Ge_4S_{10}]^{4-}$. When $n \geq 3$, the term "supertetrahedral" is used with some examples being $[In_{10}S_{20}]^{10-}$ (T3)[6], $[Cd_4In_{16}S_{35}]^{14-}$ [7], $[Zn_4In_{16}S_{33}]^{10-}$ (T4) [8] and $[In_{28}Cd_6S_{54}]^{12-}$ (T5) [9, 10]. These clusters (with $n \geq 3$) contain trivalent metals (e.g. Ga, In) or a combination of divalent and trivalent (e.g. Cd and In) ions and are always linked in three-dimensional frameworks. They have not been isolated as discrete molecular clusters. The family of compounds $K_{10}M_4Sn_4S_{17}$ (M = Mn, Fe, Co, Zn) offers the discrete supertetrahedral $[M_4Sn_4S_{17}]^{10-}$ cluster which is soluble in polar solvents where the Co and Fe analogs possess the highest solubility [11].

The $[M_4M'_4S_{17}]^{10-}$ cluster combines divalent and tetravalent metals (M: divalent and M′: tetravalent) and it features four terminal sulfide atoms, which can potentially serve as linking points to build extended frameworks. For example, we prepared $K_6Zn_4Sn_5S_{17}$ [12] a dense extended network compound composed of $[Zn_4Sn_4S_{17}]^{10-}$ clusters, linked in three dimensions by Sn^{4+} ions.

Despite its T_d point group symmetry and tetrahedral topology, the cluster does not belong to the T*n* homologous series, and in this context it represents an alternative build-

* Prof. Dr. Mercouri G. Kanatzidis
Department of Chemistry
Michigan State University
East Lansing, Michigan 48824 / USA
E-mail: kanatzidis@chemistry.msu.edu

 DOI: 10.1002/zaac.200400154

ing block for the construction of framework solids. This family of molecules has been extended to several Se analogs, prepared via solution routes, such as $K_{22}(MeOH)_{18}(H_2O)_7[Co_4(\mu_4\text{-}Se)(SnSe_4)_4]$ [13, 14]. This implies that a wider variety of members and analogs could still be made.

In this work we extended the series and scope of these cluster compounds to additional alkali, divalent and tetravalent metals. Namely, we report the synthesis, thermal stability and physicochemical properties of $K_{10}Zn_4Sn_4S_{17}$ (**I**), $K_{10}Mn_4Sn_4S_{17}$ (**II**), $K_{10}Co_4Sn_4S_{17}$ (**III**), $K_{10}Fe_4Sn_4S_{17}$ (**IV**), $Cs_{10}Cd_4Sn_4S_{17}$ (**V**) as well as the germanium analog $K_{10}Zn_4Ge_4S_{17}$ (**VI**). The compounds **V** and **VI** exhibit photoluminescence properties, and **II**, **III** and **IV** show unusual magnetic properties.

Experimental Section

Reagents

All work was done under a nitrogen atmosphere. The reagents mentioned in this study were used as obtained. Reagents: Sn and Ge were purchased from CERAC Inc., 325 mesh, 99.8 %. Sublimed sulfur was purchased from J. T. Baker Chemical Co., >99.5 %. Potassium metal, analytical reagents from Aldrich Chemical Co.; Zn, Co, Cd, Fe and Mn were purchased from Johnson Matthey/AESAR, −325 mesh, >99.5 %. Cs was from Johnson Matthey/AESAR. All reagents were stored under N_2 in a glovebox. K_2S and Cs_2S were prepared by reacting stoichiometric amounts of the elements in liquid ammonia as described elsewhere [15].

Synthesis

$K_{10}Zn_4Sn_4S_{17}$ (I). A mixture of Sn (0.5 mmol), Zn (0.5 mmol), K_2S (1.5 mmol) and S (6.0 mmol) were sealed under vacuum ($<10^{-3}$ Torr) in a silica tube and heated (at a rate of 50 °C/h) to 500 °C for 60 hours. This was followed by cooling to room temperature at 5 °C/h. The excess flux (K_2S_x) was removed with MeOH to reveal yellowish-white cubic crystals (~90 % yield based on Zn). These crystals are moderately air stable (for a few days) and need to be stored under inert atmosphere. The purity of the product was confirmed by comparison of the calculated and experimental X-ray powder diffraction patterns. Microprobe elemental analysis (EDS) with a scanning electron microscope (SEM) gave an average (five crystals were analyzed) composition of $K_{10.2}Zn_4Sn_{4.4}S_{18.2}$ which is very close to the chemical formula determined by single-crystal X-ray diffraction analysis.

$K_{10}Mn_4Sn_4S_{17}$ (II). A mixture of Sn (0.5 mmol), Mn (0.5 mmol), K_2S (2.0 mmol) and S (6.0 mmol) were sealed under vacuum ($<10^{-3}$ Torr) in a silica tube and heated (at a rate of 50 °C/h) to 650 °C for 96 hours. This was followed by cooling to room temperature at 5 °C/h. The excess flux was removed with MeOH to reveal the mixture of red cubic crystals (40 % yield based on Mn) and orange-reddish octahedral crystal (~50 %). Red cubic crystals are not air-stable, and after 4-5h deterioration could be observed. Powder XRD analysis revealed the orange octahedral crystals are K_2MnSnS_4[16]. The SEM/EDS average composition of the red cubic crystals was $K_{10.7}Mn_4Sn_{4.6}S_{18.9}$. All attempts to prepare pure phase of $K_{10}Mn_4Sn_4S_{17}$ without any traces of K_2MnSnS_4 failed.

$K_{10}Co_4Sn_4S_{17}$ (III). A mixture of Sn (2.0 mmol), Co (2.0 mmol), K_2S (2.5 mmol) and S (6.0 mmol) were sealed under vacuum ($<10^{-3}$ Torr) in a silica tube and heated (at a rate of 50 °C/h) to 650 °C for 60 hours. This was followed by cooling to room temperature at 5 °C/h. Dark (almost black) crystals were recovered (~90 % yield based on Co). These crystals are moderately air stable (for a few days). The purity of the product was confirmed by comparison of the calculated and experimental X-ray powder diffraction patterns. SEM/EDS indicated an average composition of $K_{10.7}Co_{3.8}Sn_4S_{16.8}$.

$K_{10}Fe_4Sn_4S_{17}$ (IV). Minor glass attack was observed during synthesis of this compound. To prevent this attack, carbon coated silica ampoules were used. $K_{10}Fe_4Sn_4S_{17}$ was synthesized by the direct reaction from a mixture of 0.119 g (1 mmol) of Sn, 0.058 g (1 mmol) of Fe, 0.138 g (1.25 mmol) of K_2S and 0.096 g (3 mmol) of S. The reagents were mixed, sealed in an evacuated silica tube, and heated at 650 °C for 60 h. This was followed by cooling to room temperature at 5 °C/h. Black crystals were recovered from the ampoule in >90 % yield (based on Fe). The purity of the product was confirmed by comparison of the calculated and experimental X-ray powder diffraction patterns. These crystals decompose after a few days in air. EDS analysis on the several crystals gave an average composition of $K_{9.9}Fe_{4.2}Sn_4S_{17.0}$.

$Cs_{10}Cd_4Sn_4S_{17}$ (V). This compound was synthesized from a mixture of 0.036 g (0.3 mmol) of Sn, 0.034 g (0.3 mmol) of Cd, 0.447 g (1.5 mmol) of Cs_2S and 0.115 g (3.6 mmol) of S. The reagents were mixed, sealed in an evacuated silica tube, and heated at 500 °C for 4 days. This was followed by cooling to room temperature at 5 °C/h. The excess flux was removed with MeOH to reveal yellowish-white transparent rectangular crystals in >95 % yield. EDS analysis on several crystals gave an average composition of $Cs_{10.2}Cd_{4.1}Sn_4S_{17.2}$. The crystals appear to be air-stable.

$K_{10}Zn_4Ge_4S_{17}$ (VI). This compound was synthesized from a mixture of 0.037 g (0.5 mmol) of Ge, 0.032 g (0.5 mmol) of Zn, 0.275 g (2.5 mmol) of K_2S and 0.193 g (6 mmol) of S. The reagents were mixed, sealed in an evacuated silica tube, and heated at 500 °C for 4 days. This was followed by cooling to room temperature at 5 °C/h. The excess flux was removed with MeOH to reveal yellow-brown transparent rectangular crystals in ~90 % yield (some ZnS was also present ~8-10 %). EDS analysis on several crystals gave an average composition of $K_{10.8}Zn_{4.3}Ge_4S_{16.7}$. The crystals are air-sensitive.

Physical property measurements

Powder X-ray Diffraction. Powder diffraction measurements were performed on a CPS 120 INEL X-ray diffractometer using monochromatized Cu Kα (λ = 1.54049 Å) radiation and equipped with a position-sensitive detector. Samples were ground and spread on a glass slide (compound **II** and **VI** were prepared in a glove box and covered with mineral oil).

Microprobe Analyses. The analyses were performed using a JEOL JSM-6400V scanning electron microscope (SEM) equipped with a Tracor Northern energy dispersive spectroscopy (EDS) detector. Data acquisition was performed with an accelerating voltage of 20 kV and 30 s accumulation time.

Differential Thermal Analysis (DTA). DTA experiments were performed on a computer-controlled Shimadzu DTA-50 thermal analyzer. Typically a sample (~25 mg) of ground crystalline material was sealed in a quartz ampoule under vacuum. A quartz ampoule of equal mass filled with Al_2O_3 was sealed and placed on the refer-

Table 1 Data for crystal structure analysis for $K_{10}Zn_4Sn_4S_{17}$ (**I**), $K_{10}Mn_4Sn_4S_{17}$ (**II**).

Identification code	**I**	**II**
Empirical formula	$K_{10}Zn_4Sn_4S_{17}$	$K_{10}Mn_4Sn_4S_{17}$
Formula weight	1672.26	1630.54
Temperature	293(2) K	293(2) K
Wavelength	0.71073 Å	0.71073 Å
Crystal system	cubic	cubic
Space group	$F\bar{4}3c$ (No. 219)	$P\bar{4}3m$ (No. 215)
Unit cell dimensions	a = 19.923(3) Å	a = 10.064(2) Å
Volume	7907.7(19)	1019.5(4)
Z	8	1
Density (calculated)	2.809 g/cm^3	2.656 g/cm^3
Absorption coefficient	6.821 mm^{-1}	5.499 mm^{-1}
F(000)	6256	762
Theta range for data collection	1.35 to 28.18 deg	2.07 to 28.25 deg
Reflections collected	16593	2947
Independent reflections	818 [R(int) = 0.0410]	483 [R(int) = 0.0525]
Completeness to theta = 28.14	99.80 %	95.60 %
Goodness-of-fit on F^2	1.499	1.114
Final R indices [I>2σ(I)]	R1 = 0.0441, wR2 = 0.1122	R1 = 0.0209, wR2 = 0.0422
R indices (all data)	R1 = 0.0709, wR2 = 0.1228	R1 = 0.0282, wR2 = 0.0450
Absolute structure parameter	0.07(8)	0.44(5)
Largest diff. peak and hole	1.651 and −1.843 e.Å^{-3}	0.497 and −0.608 e.Å^{-3}

Note. $R1 = \Sigma(|F_{obs}| - |F_{calc}|)/\Sigma(F_{obs})$;
$wR2 = \Sigma\{[w(F_{obs}^2 - F_{calc}^2)^2/\Sigma[w(F_{obs}^2)^2]\}^{1/2}$, $w = 1/[\sigma^2F_{obs}^2 + 151.11P]$,
$P = (F_{obs}^2 + 2F_{calc}^2)/3$.

ence side of the detector. The sample was heated to the desired temperature at 10 °C/min, then isothermed for 10 min, and finally cooled to 50 °C at the same rate. The residue of the DTA experiment was examined by X-ray powder diffraction. To evaluate congruent melting, we compared the X-ray powder diffraction patterns before and after the DTA experiments, as well as monitored the stability/reproducibility of the DTA diagrams upon cycling under the above conditions at least two times.

Diffuse reflectance UV/Vis/Near-IR spectroscopy. Optical diffuse reflectance measurements were performed at room temperature using a Shimadzu UV-3101PC double-beam spectrophotometer. The instrument is equipped with an integrating sphere and controlled by a personal computer. $BaSO_4$ was used as a 100 % reflectance standard. The sample was prepared by grinding the crystals to a powder and spreading it on a compacted surface of the powdered standard material, preloaded into a sample holder. The reflectance versus wavelength data generated was used to estimate the band gap of the material by converting reflectance to absorption data using Kubelka-Munk function as described in the reference [17].

Single-crystal VIS spectroscopy. Optical transmission measurements were made at room temperature on single crystals using a Hitachi U-6000 microscope FT spectrophotometer with an Olympus BH-2 metallurgical microscope over a range of 400-900 nm. The crystals were placed on the glass slide and covered with mineral oil for the measurements.

Photoluminescence spectroscopy. Photoluminescence spectra were obtained on a SPEX Fluorolog-2, Model F111A1 spectrofluorimeter. Excitation wavelengths were chosen from a 150-W xenon arc lamp by means of a single grating spectrometer. This spectrometer was equipped with a 1200 groove/mm diffraction grating and 5-nm band-pass slits. The sample compartment was equipped with a vertically mounted liquid nitrogen Dewar. Emitted light was collected in the "front face" mode, 22.5° away from the incident beam. Emission wavelengths were selected with a single grating spectrometer, equipped with a 1200 groove/mm diffraction grating and 1.0-nm band-pass slits. The signal was detected with a Hamamatsu R928 photomultiplier. Excitation spectra were corrected for lamp intensity by comparison with a quantum counter reference detector loaded with Rhodamine B. Powdered samples were loaded in 3-mm silica tubes and sealed under vacuum (approximately 1.0* 10^{-4} mbar).

Cathodoluminescence spectroscopy. The analyses were performed at room temperature using a JEOL JSM-6300F Field Emission Scanning Electron Microscope (SEM) equipped with Gatan MonoCL SP high-performance cathodoluminescence system. Data acquisition was carried out with an accelerating voltage of 10 kV and the spectrum was acquired in 200-800 nm range. For each compound luminescence was measured on five single crystals.

Magnetic measurements. The magnetization of the polycrystalline samples of $K_{10}Mn_4Sn_4S_{17}$ (**II**), $K_{10}Co_4Sn_4S_{17}$ (**III**) and $K_{10}Fe_4Sn_4S_{17}$ (**IV**) were measured on a Quantum Design SQUID magnetometer at a field of 0.01 Tesla over the temperature range of 2-400 K. The data were corrected for holder and for ion-core diamagnetism. Magnetization versus temperature measurements was performed after zero-field cooling (ZFC) and field cooling (FC).

Solid-state NMR. The room temperature solid-state NMR data were taken on a 9.4 T Varian Infinity Plus NMR spectrometer using a double resonance magic angle spinning (MAS) probe. Samples (~ 100 mg) were spun at frequencies between 6 and 8 kHz using zirconia rotors of 6 mm outer diameter. Bloch decay spectra were taken with the excitation/detection channel tuned to ^{119}Sn at 148.67 MHz, a 3.5 μs 90° pulse (calibrated to ± 0.1 μs with $Sn(CH_3)_4$), and a relaxation delay between 0.001 and 2000 s. Chemical shifts (CS) were referenced to $Sn(CH_3)_4$ at 0 ppm. The spin-lattice relaxation time (T_1) of a compound is estimated from the exponential buildup of signal intensity as a function of relaxation delay. Chemical shift anisotropy (CSA) principal values were derived from Herzfeld-Berger fitting of the MAS isotropic and sideband intensities. For a given compound, CSA principal value fitting was done for spectra at two different MAS frequencies.

Table 2 Data for crystal structure analysis for $K_{10}Co_4Sn_4S_{17}$ (**III**) and $K_{10}Fe_4Sn_4S_{17}$ (**IV**)

Identification code	**III**	**IV**
Empirical formula	$K_{10}Co_4Sn_4S_{17}$	$K_{10}Fe_4Sn_4S_{17}$
Formula weight	1646.5	1634.18
Temperature	293(2) K	293(2) K
Wavelength	0.71073 Å	0.71073 Å
Crystal system	cubic	cubic
Space group	$P\bar{4}3m$ (No. 215)	$P\bar{4}3m$ (No. 215)
Unit cell dimensions	a = 9.9332(13) Å	a = 9.9756(12) Å
Volume	980.1(2)	992.7(2) $Å^3$
Z	1	1
Density (calculated)	2.790 g/cm^3	2.734 g/cm^3
Absorption coefficient	6.124 mm^{-1}	5.837 mm^{-1}
F(000)	770	766
Theta range for data collection	1.35 to 28.18 deg	2.07 to 28.25 deg
Reflections collected	9422	9739
Independent reflections	497 [R(int) = 0.0183]	507 [R(int) = 0.0303]
Goodness-of-fit on F^2	1.183	1.192
Final R indices [I>2σ(I)]	R1 = 0.0088,wR2 = 0.0211	R1 = 0.0177, wR2 = 0.0401
R indices (all data)	R1 = 0.0090,wR2 = 0.0211	R1 = 0.0200, wR2 = 0.0410
Absolute structure parameter	0.045(19)	0.02(4)
Largest diff. peak and hole	0.255 and −0.178 e.$Å^{-3}$	0.386 and −0.455 e.$Å^{-3}$

Note. $R1 = \Sigma(|F_{obs}| - |F_{calc}|)/\Sigma(F_{obs})$;
$wR2 = \Sigma\{[w(F_{obs}^2 - F_{calc}^2)^2/\Sigma[w(F_{obs}^2)^2]\}^{1/2}$, $w = 1/[\sigma^2F_{obs}^2 + 151.11P]$,
$P = (F_{obs}^2 + 2F_{calc}^2)/3$.

Single-crystal X-ray crystallography

A Siemens SMART Platform CCD diffractometer operating at room temperature and using graphite-monochromatized Mo Kα radiation, was used for data collection.

$K_{10}Zn_4Sn_4S_{17}$ (I). A cubic-shaped crystal with dimensions 0.083 mm x 0.092 mm x 0.088 mm was chosen for single crystal diffraction and was mounted at the end of a glass fiber. A full sphere of data were collected, with scans of 0.3 deg steps in ω in groups of 606, 435, 606, and 435 frames at ϕ settings of 0, 90, 180, and 270 and exposure time of 30 s/frame. Cell refinement and data reduction were carried out with the program SAINT [18]. An empirical absorption correction was done to the data using SADABS [19]. The space group was determined from systematic absences and intensities were extracted by the program XPREP [19]. The structure was solved with direct methods using SHELXS and least square refinement was done against F^2 using routines from SHELXTL software [19]. In this compound no disorder was observed, but the 6g site had only 50 % occupancy of K3 atom.

$K_{10}Mn_4Sn_4S_{17}$ (II). A polyhedral shaped crystal with dimensions 0.064 mm x 0.080 mm x 0.110 mm was mounted on the end of glass fiber. A half-sphere of data were collected with 0.3 deg steps in ω and at ϕ settings of 0 and 90 deg and exposure time of 20 s/frame. All collection parameters and data treatment procedures were analogous to compound **I**. In this compound no disorder was observed, but the 6g site had only 50 % occupancy of K3 atom.

$K_{10}Co_4Sn_4S_{17}$ (III). A polyhedral-shaped crystal with dimensions 0.071 mm x 0.129 mm x 0.056 mm was mounted at the end of a glass fiber. All collection parameters and data treatment procedures were analogous to compound **I**. The 6g site was found to be only half occupied by the K3 atom. Anisotropic refinement of this atom revealed that the thermal displacement parameter was much higher along one direction. A disordered model was considered for this atom, with two new partially occupied K3 and K33 atoms, with occupancy of 19 % and 31 % respectively.

$K_{10}Fe_4Sn_4S_{17}$ (IV). A crystal with dimensions 0.042 mm x 0.055 mm x 0.110 mm was mounted on a glass fiber. All collection parameters and data treatment procedures were the same as in compound **I**.Two K atoms were found to be partially occupied: atom K1 in the 12i position had 33 % occupancy, and K3 atom in the 6f position had 50 % occupancy. Anisotropic refinement of the K3 atom revealed that it has elevated thermal displacement parameter along the b-direction. A split site was modeled for this atom, which resulted in a drop of the R1 value from 0.042 to 0.035. Similar phenomenon was observed also for the K1 atom.

$Cs_{10}Cd_4Sn_4S_{17}$ (V). A polyhedral-shaped crystal with dimensions 0.140 mm x 0.110 mm x 0.080 mm was mounted at the end of a glass fiber. All collection parameters and data treatment procedure were as stated above. Based on the observed systematic absences the space groups P4/mbm, P-4b2, P-4m2 and P-4 were possible. Structure solution and refinement were attempted in all space groups but satisfactory refinement was achieved only in P-4. After extinction correction and anisotropic refinement (R1=0.0361) two high intensity peaks remained in the electron density map: 10.9 e/$Å^3$ near atom Cs7 and 3.1 e/$Å^3$ near atom Cs1. A disordered model was considered for these atoms (occupancy factor of Cs1 was 96.9 % and of Cs 7 50.0 %) and after refinement with anisotropic thermal displacement parameters, the R1 value dropped to 0.0192.

$K_{10}Zn_4Ge_4S_{17}$ (VI). A cubic yellow crystal with dimensions of 0.05 x 0.05 x 0.05 mm of $K_{10}Zn_4Ge_4S_{17}$ was mounted on a glass fiber. The data collection was conducted at 173 K. All collection parameters and data treatment procedure were analogous to the compound **I**. The systematic absences pointed to the two possible space groups: P-43m (no. 215) and Pm-3m (no. 221). Attempts to solve the structure in the centrosymmetric Pm-3m failed.On the other hand the structure could be smoothly solved in P−43m space group (non-centrosymmetric). A search for possible missed symmetry done with the program Platon [20] revealed no such symmetry validating the chosen space group. After initial location of all atoms was found, the R1 value dropped to 0.0591. The value of the Flack parameter (0.041) suggested that the correct absolute structure was chosen for refinement. After refining all atoms anisotropically and turning on extinction correction, the R1 decreased to 0.0259. The residual difference Fourier map was featureless.

Table 3 Data for crystal structure analysis for $Cs_{10}Cd_4Sn_4S_{17}$ (**V**) and $K_{10}Zn_4Ge_4S_{17}$ (**VI**).

Identification code	**V**	**VI**
Empirical formula	$Cs_{10}Cd_4Sn_4S_{17}$	$K_{10}Zn_4Ge_4S_{17}$
Formula weight	2798.48	1487.86
Temperature	293(2) K	153(2) K
Wavelength	0.71073 Å	0.71073 Å
Crystal system	tetragonal	cubic
Space group	$P\bar{4}$ (no. 81)	$P\bar{4}3m$ (no. 215)
Unit cell dimensions	a = 15.046(3) Å c = 10.534(3) Å	a = 9.817(4) Å
Volume	2384.8(10) Å^3	946.0(6) Å^3
Z	2	1
Density (calculated)	3.897 g/cm^3	2.612 g/cm^3
Absorption coefficient	12.077 mm^{-1}	7.664 mm^{-1}
F(000)	2428	710
Theta range for data collection	1.35 to 28.18 deg	2.07 to 28.25 deg
Reflections collected	21466	2733
Independent reflections	5490 [R(int) = 0.0255]	469 [R(int) = 0.0391]
Goodness-of-fit on F^2	1.166	0.998
Final R indices [I>2σ(I)]	R1 = 0.0192, wR2 = 0.0433	R1 = 0.0259, wR2 = 0.0488
R indices (all data)	R1 = 0.0220, wR2 = 0.0440	R1 = 0.0338, wR2 = 0.0508
Absolute structure parameter	0.336(17)	0.04(3)
Largest diff. peak and hole	1.163 and −0.871 e.Å^{-3}	0.527 and −0.678 e.Å^{-3}

Note. $R1 = \Sigma(|F_{obs}| - |F_{calc}|)/\Sigma(F_{obs})$;
$wR2 = \Sigma\{[w(F_{obs}^2 - F_{calc}^2)^2/\Sigma[w(F_{obs}^2)^2]\}^{1/2}$, $w = 1/[\sigma^2F_{obs}^2 + 151.11P]$,
$P = (F_{obs}^2 + 2F_{calc}^2)/3$.

Since the X-ray scattering factors of Zn and Ge are similar it is difficult to distinguish them. Nevertheless, interchanging their positions in the cluster as well as a modeling of the substitutional replacement gave higher R1 value (R1=0.038 and 0.0341 respectively).

Details of the crystal data and refinement are summarized in Tables 1, 2 and 3. Atomic coordinates and equivalent isotropic displacement parameters are given in the Table 4−5. A complete table of crystallographic data and anisotropic displacement parameters for all compounds are deposited as Supporting Information.

Results and Discussion

Synthesis

In Table 7 we summarize the optimized reaction conditions for the preparation of all compounds described.We found that several factors influence the outcome of the reaction: basicity of flux, temperature, alkali counter-ion size, and the nature of the divalent metal. The influences of these are presented below.

One of the main advantages of polychalcogenide fluxes is the ease with which Lewis basicity could be changed, simply by altering the K_2S/S (or Cs_2S/S) ratio. This ratio influences the melting point of the flux and the size of the polysulfide chains that are formed in it [21, 22]. High K_2S/S ratios result in shorter polysulfide chains and higher Lewis basicity. It was found that reactions conducted at high K_2S/S ratio (e.g. 10/12, 8/12) led to binary phases, such as SnS_2. Decreasing the ratio in the range of 6/12 − 3/12, resulted in the $A_{10}M_4M'_4S_{17}$ phase with some binary or ternary impurities (e.g. $K_2Sn_2S_5$). Relatively pure phase could be prepared only in this ratio region. Further decrease of the K_2S/S ratio to 2/12 − 1/12 resulted in ternary compounds and sulfur. Generally, crystals obtained from reactions conducted at 650 °C, were larger and better formed than crystals from the same reaction conducted at 400 °C. Temperatures >650 °C resulted in binary phases, as the main products

Table 4 Atomic coordinates and equivalent isotropic displacement parameters (Å^2 x 10^3) for $K_{10}Zn_4Sn_4S_{17}$ (**I**), $K_{10}Mn_4Sn_4S_{17}$ (**II**) and $K_{10}Co_4Sn_4S_{17}$ (**III**). U(eq) is defined as one third of the trace of the orthogonalized U^{ij} tensor.

Atom	Wyckoff position	Occup.	X	Y	Z	U(eq)
			$K_{10}Zn_4Sn_4S_{17}$ (**I**)			
Sn	32e		0.3879(1)	0.3879(1)	0.3879(1)	19(1)
Zn	32e		0.0670(9)	0.0671(1)	0.0670(9)	21(1)
S1	8a		0	0	0	15(2)
S2	96h		0.0033(2)	0.1407(8)	0.1330(8)	29(1)
S3	32e		0.3203(8)	0.3204(2)	0.3204(2)	47(2)
K1	32e		0.1656(8)	0.1657(2)	0.1657(2)	65(2)
K2	24d		0.2500	0	0	40(2)
K3	48g	0.5	0.0247(5)	0.2500	0.2500	45(3)
			$K_{10}Mn_4Sn_4S_{17}$ (**II**)			
Sn	4e		0.7733(3)	0.7733(3)	0.7733(3)	23(1)
Mn	4e		0.1360(8)	0.1360(8)	0.1360(8)	25(1)
S1	1a		0	0	0	20(1)
S2	12i		0.2767(7)	0.2767(7)	0.0011(7)	38(1)
S3	4e		0.6394(4)	0.6394(4)	0.6394(4)	63(1)
K1	3d		1/2	0	0	45(1)
K2	4e		0.3344(9)	0.3344(9)	0.3344(9)	97(1)
K3	6g	0.5	0.0562(4)	1/2	1/2	40(1)
			$K_{10}Co_4Sn_4S_{17}$ (**III**)			
Sn	4e		0.2236(1)	0.2236(1)	0.2236(1)	19(1)
Co	4e		0.8664(9)	0.8664(9)	0.8664(9)	20(1)
S1	12i		0.2720(2)	0.2720(2)	0.9926(1)	32(1)
S2	4e		0.3589(4)	0.3589(4)	0.3589(4)	47(1)
S3	1a		0	0	0	17(1)
K1	3d		1/2	0	0	40(1)
K2	4e		0.6682(4)	0.6682(4)	0.6682(4)	64(1)
K3	6g	0.187	0.0249(1)	1/2	1/2	28(1)
K33	6g	0.31	0.0614(1)	1/2	1/2	28(1)

$U^{ij} = {}^1/_3(4\pi)^{-2}\,(a^2\beta_{11}+b^2\beta_{22}+c^2\beta_{33}+ab(\cos\gamma)\beta_{12}+ac(\cos\beta)\beta_{13}+bc(\cos\alpha)\beta_{23})$.

Table 5 Atomic coordinates (x 10^4) and equivalent isotropic displacement parameters (Å^2 x 10^3) for $K_{10}Fe_4Sn_4S_{17}$ (**IV**) and $Cs_{10}Cd_4Sn_4S_{17}$ (**V**).

Atom	Wyckoff position	Occup.	X	Y	Z	U(eq)
			$K_{10}Fe_4Sn_4S_{17}$ (**IV**)			
Sn1	4e		0.2749(4)	0.2749(4)	0.2749(4)	27(1)
Fe2	4e		0.6342(7)	0.6342(7)	0.6342(7)	27(1)
S1	1b		1/2	1/2	1/2	19(1)
S2	12i		0.2276(3)	0.2276(3)	0.5058(3)	42(1)
S3	4e		0.1403(4)	0.1403(4)	0.1403(4)	72(1)
K1	12i	0.33	0.1543(1)	0.1543(1)	0.8108(1)	77(5)
K2	3c		0	1/2	1/2	48(1)
K3	6f	0.5	0.4486(1)	0	0	64(1)
			$Cs_{10}Cd_4Sn_4S_{17}$ (**V**)			
Sn1	4h		0.4952(1)	0.2782(2)	0.2199(9)	20(1)
Sn2	4h		0.0047(7)	0.7782(2)	0.2200(1)	20(1)
Cd1	4h		0.3675(4)	0.5058(4)	0.1354(3)	24(1)
Cd2	4h		0.1324(8)	0.0058(6)	0.1354(1)	24(1)
Cs1	4h	0.97	0.2756(3)	0.2243(4)	0.5000(2)	37(1)
Cs11	4h	0.03	0.2374(1)	0.2627(1)	0.5005(1)	37(1)
Cs2	1d		1/2	1/2	1/2	33(1)
Cs3	1b		0	0	1/2	33(1)
Cs4	4h		0.1692(2)	0.4806(3)	0.3325(6)	48(1)
Cs5	4h		0.0193(5)	0.3307(9)	0.6675(1)	48(1)
Cs6	4h		0.2494(3)	0.2505(7)	0.0000(1)	35(1)
Cs7	2g	0.5	0.0000(1)	1/2	0.9705(1)	43(1)
Cs77	2g	0.5	0.0000(1)	1/2	0.02950(1)	43(1)
S1	4h		0.3667(1)	0.3662(1)	0.2700(2)	26(1)
S2	4h		0.1337(5)	0.1332(7)	0.7299(6)	26(1)
S3	1a		0	0	0	19(1)
S4	4h		0.4968(8)	0.2302(9)	0.0026(9)	27(1)
S5	4h		0.0031(1)	0.7303(2)	0.0024(8)	28(1)
S6	1c		1/2	1/2	0	19(1)
S7	4h		0.1297(9)	0.1435(1)	0.2721(1)	28(1)
S8	4h		0.6298(1)	0.3564(1)	0.2724(4)	28(1)
S9	4h		0.4844(1)	0.1493(2)	0.3446(5)	40(1)
S10	4h		0.0156(1)	0.6492(6)	0.3446(8)	40(1)

Table 6 Atomic coordinates (x 10^4) and equivalentisotropic displacement parameters (Å^2 x 10^3) for $K_{10}Zn_4Ge_4S_{17}$ (**VI**).

Atom	Wyckoff position	Occup.	X	Y	Z	U(eq)
			$K_{10}Zn_4Ge_4S_{17}$ (**VI**)			
K1	12h		0.1250(1)	1/2	1/2	33(1)
K2	6g		0.0473(7)	1/2	1/2	68(1)
K3	4e	0.5	0.6692(1)	0.6692(1)	0.6692(1)	38(1)
Ge	4e		0.2234(5)	0.2234(5)	0.2234(5)	17(1)
Zn	4e		0.8662(8)	0.8662(8)	0.8662(8)	20(1)
S1	12i		0.2721(2)	0.2721(2)	0.0053(7)	45(1)
S2	4e		0.3513(4)	0.3513(4)	0.3513(4)	14(1)
S3	1a		0	0	0	26(1)

Table 7 Optimized reaction conditions for preparation of compounds **I-VI**.

Compound	Method	Sn or Ge	M	K_2S or Cs_2S	S	Isothermal step: Temp/time
$K_{10}Mn_4Sn_4S_{17}$	flux	1	1	4	12	500 °C/96h
$K_{10}Fe_4Sn_4S_{17}$	Direct combination	1	4	5	12	650 °C/60h
$K_{10}Co_4Sn_4S_{17}$	Direct combination	1	4	5	12	650 °C/60h
$K_{10}Zn_4Sn_4S_{17}$	flux	1	1	3	12	500 °C/60h
$Cs_{10}Cd_4Sn_4S_{17}$	flux	1	1	5	12	650 °C/60h
$K_{10}Zn_4Ge_4S_{17}$	flux	1	1	5	12	500 °C/96h

(except in the case of **I**). The flux reaction chemistry did not produce $K_{10}M_4Sn_4S_{17}$ when M was Fe or Co, giving only the binary FeS_2, CoS_2 and SnS_2. Compounds **I** and **VI** could be prepared by either flux or direct reactions, but the flux medium is superior for crystal growth relatively to direct solid-state reactions, see Figure 1.

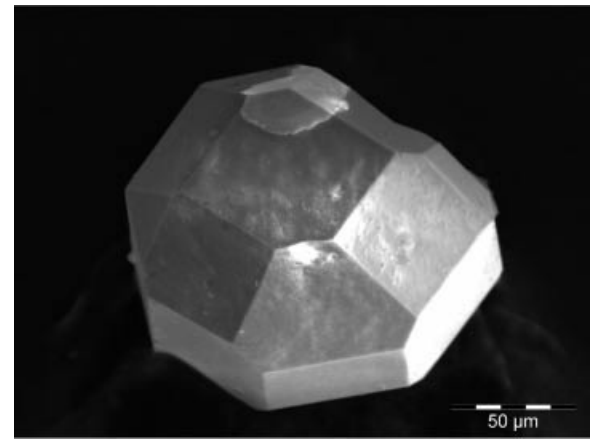

Figure 1 SEM image of a typical single crystal of $Cs_{10}Cd_4Sn_4S_{17}$.

The divalent metals with strong tetrahedral coordination preference seem to stabilize the $[M_4Sn_4S_{17}]^{10-}$ cluster motif. Reactions with Ni at various K_2S/S ratios, (from 1/12 to 10/12, at 450, 500 and 650 °C) did not give quaternary phases or even ternary ones. The products of these reactions were NiS, NiS_2 and binary tin sulfides. Because Mg^{2+} can adopt tetrahedral coordination, we also attempted reactions with Mg as a possible replacement for the divalent M atom. These experiments were unsuccessful with binary sulfides as the major products.

The counter-ion size seems to be important in stabilizing the $A_{10}M_4M'_4S_{17}$ structure. When A = K and Cs (and presumably Rb) the cluster forms readily, however with Li and Na no cluster compound could be isolated. Instead, different phases with extended layered and three-dimensional structures formed [23].

The first row transition metals used in this study (Mn, Fe, Co and Zn) have ionic radii (in +2 oxidation state) in the range of 0.6-0.67 Å. For these metals the size of K^+ is evidently large enough to stabilize cluster in the crystal structure. But when Cd^{2+} (ionic radius 0.84 Å) was used, aiming to prepare $K_{10}Cd_4Sn_4S_{17}$, the expected structure did not form. Instead the layered K_2CdSnS_4 was produced [21]. It is possible that the larger Cd^{2+} ion leads to a larger cluster, which cannot be stabilized by K^+ ions leading to structural collapse. In order to check this hypothesis, we switched to the larger Cs^+ cation (to compensate for the larger cluster) which indeed gave $Cs_{10}Cd_4Sn_4S_{17}$ (see Table 3). The counterion effect appears to be important in the stabilization of the Se analogs as well, which of course are larger than the sulfide analogs. The selenide clusters are stabilized with the bulky complex cations, such as $[K_{10}(H_2O)_{16}(MeOH)_{0.5}]^{10+}$ and $[K_{22}(MeOH)_{18}(H_2O)_7]^{10+}$ [13, 14].

DTA experiments in conjunction with X-ray diffraction showed that compounds **I** and **VI** melt congruently at 820

and 656 °C respectively. For **II** no DTA measurements were done because it always was obtained admixed with K_2MnSnS_4. Compound **III** decomposes at 704 °C giving CoS_2 as one of the products. Compound **IV** decomposes at 661 °C to FeS_2. For compound **V** decomposition occurs at 714 °C and the main phase after decomposition was CdS.

Solubility of compounds I-VI

A potential use of the molecular compounds described in this article would be their application as precursors for mesoporous materials. Because the synthesis of mesoporous phases typically occurs in solution, we conducted an evaluation of the solubility of these compounds in several relevant solvents normally used for the synthesis of mesoporous materials, such as water and formamide. The solubility in both water and formamide was as follows:

$$K_{10}Co_4Sn_4S_{17} > K_{10}Zn_4Ge_4S_{17} > K_{10}Fe_4Sn_4S_{17} > K_{10}Mn_4Sn_4S_{17} \cong Cs_{10}Cd_4Sn_4S_{17} > K_{10}Zn_4Sn_4S_{17}$$

The Co analog was the most soluble. In general the solubility of all compounds was much lower in formamide than in water.

Preliminary experiments for the evaluation of the stability of compounds **I-VI** in solution were done by measuring the time periods from the total dissolution of the compound to the visual observation of a precipitate. The Zn analog was found to be the most stable in solution. The stability of compounds **I-VI** in aqueous solution decreases in the following order (from left to right):

$$K_{10}Zn_4Sn_4S_{17}\ (6\ min) \cong K_{10}Co_4Sn_4S_{17}\ (5\text{-}6\ min) > K_{10}Fe_4Sn_4S_{17}\ (3\ min) >> Cs_{10}Cd_4Sn_4S_{17}\ (1.5\text{-}2\ min) > K_{10}Mn_4Sn_4S_{17} \cong K_{10}Zn_4Ge_4S_{17}\ (few\ seconds)$$

In brackets are the time periods after which precipitation was observed.

Preliminary results using $K_{10}Co_4Sn_4S_{17}$ as a starting material to prepare mesostructured materials are encouraging, and will be published later.

Structure of $A_{10}M_4M'_4S_{17}$ (A = K, Cs; M = Mn, Co, Zn, Fe or Cd; M′ = Sn or Ge)

All six compounds have the discrete molecular $[M_4M'_4S_{17}]^{10-}$ clusters, which are well separated by alkali cations (see Figure 2). The cluster has an ideal tetrahedral symmetry T_d and practically functions as a huge tetrahedral ES_4^{10-} ($E = M_4Sn_4S_{13}$) structural unit. A four-coordinated sulfur atom (μ_4-S) is located at the center of the cluster. This atom is bonded to four divalent metal ions (Mn, Co, Zn, Fe or Cd) forming a $[M_4S]^{6+}$ tetrahedral core (see Figure 3). The μ_4-S-M bonds are shorter than the average M-S bond see Table 5, and this is well known for tetrahedrally connected sulfur [24]. The angle M-μ_4S-M in the $[M_4S]^{6+}$ cation is ideally tetrahedral. The $[M_4S]^{6+}$ moiety is capped

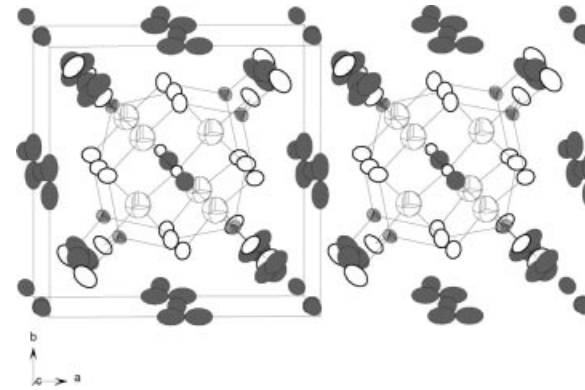

Figure 2 ORTEP representation of the unit cell of **IV**. White open spheres are S atoms; White octant spheres are Fe atoms; gray octant spheres are Sn atoms and gray spheres are K atoms.

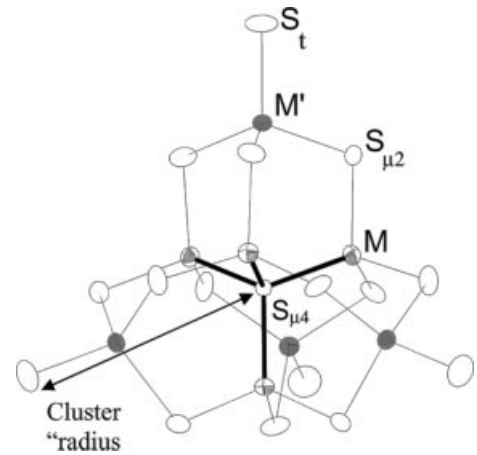

Figure 3 ORTEP representation and labeling scheme for a $[M_4M'_4S_{17}]^{10-}$ cluster (M = Zn, Mn, Co, Fe, Cd; M′ = Sn, Ge).

with four tridentate $[SnS_4]^{4-}$ (or $[GeS_4]^{4-}$) fragments to complete the structure of the cluster. In this fashion, three sulfur atoms (μ_2-S) of the $[SnS_4]^{4-}$ unit are coordinated to metal ions of the $[M_4S]^{6+}$ fragment, whereas the forth sulfur atom remains terminal (S_t) interacting with the alkali ions. The S_t-Sn distance is shorter than the average Sn-S bond.

In compounds **I-IV** and **VI** there are three different K^+ sites. Three K(1) atoms interact with terminal S_t atoms forming a pyramid. The three K atoms define the base of the pyramid but because of fractional occupancies and disorder in these atoms there is also another set of closely lying K atoms that define the base of another slightly rotated base. The K-S distances of 3.080-3.210 Å. The μ_2-S atoms interact with two K1, one K2 and one K3 ions at distances in the range of 3.23-3.65 Å (see Figure 4a). The K3 atom in $K_{10}Co_4Sn_4S_{17}$ was modeled as a split site with 50 % occupancy. Due to the lower crystal symmetry of $Cs_{10}Cd_4Sn_4S_{17}$ seven different Cs^+ ions are present in the structure. For two of them, Cs1 and Cs7, a split site occupancy model was used. S_t is surrounded by three Cs atoms (Cs4 and two Cs5)

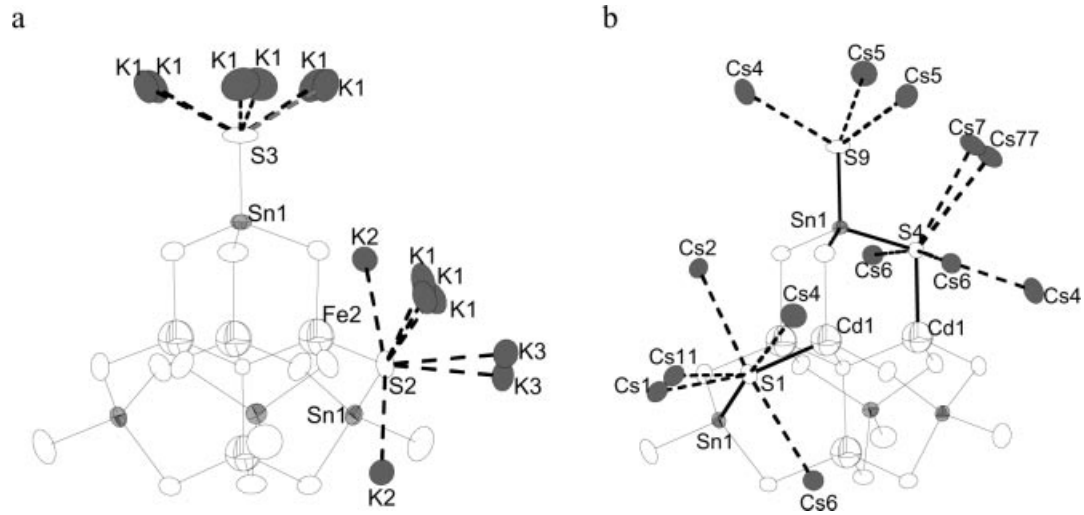

Figure 4 (a) Coordination environment of S_t (S3) and μ_2S (S2) in **IV**, (b) coordination environment of S_t (S9) and μ_2S (S4 and S1) in **V**. Non-covalent interactions are shown as a dashed lines.

Table 8 Selected distances /Å and angles /deg for $A_{10}M_4M'_4S_{17}$ (**I-VI**).

	I (M=Zn, M′=Sn)	**II** (M=Mn, M′=Sn)	**III** (M=Co, M′=Sn)	**IV** (M=Fe, M′=Sn)	**V** (M=Cd, M′=Sn)	**VI** (M=Zn, M′=Ge)
μ_4S-M	2.315 (2)	2.372(1)	2.297(0)	2.320(1)	2.453(1)	2.274(1)
M-μ_4S-M	109.47(7)	109.47(2)	109.47(1)	109.47(2)	109.77(2)	109.47(1)
μ_2S-M	2.345(4)	2.419(1)	2.314(1)	2.332(1)	2.524(1)	2.357(1)
μ_2S-M′	2.406(4)	2.401(1)	2.393(1)	2.398(1)	2.402(2)	2.245(1)
S_t-M′	2.329(4)	2.334(3)	2.328(1)	2.326(1)	2.349(2)	2.175(1)
μ_2S-M′-μ_2S	110.61(3)	110.91(3)	110.18(2)	109.84(3)	110.84(5)	111.14(1)
S_t-M′-μ_2S	108.31(14)	107.99(5)	108.75(2)	109.10(4)	106.63(6)	107.75(1)
M-M	3.781(3)	3.873(1)	3.751(1)	3.788(1)	3.990(1)	3.713(1)
μ_2S-A (A=K^+ or Cs^+)	3.215(4)	3.2254(16)	3.2072(7)	3.5415(4)	3.4774(14)	3.485(1)
	3.235(4)	3.2295(17)	3.2747(9)	3.2617(13)	3.6621(19)	3.399(1)
	3.430(4)	3.454(3)	3.3295(11)	3.213(10)	3.7358(16)	3.199(1)
	3.647(4)	3.5787(8)	3.5263(5)		3.8110(16)	3.206(1)
S_t-A (A=K^+ or Cs^+)	3.108(6)	3.091(3)	3.0960(10)	2.982(6)	3.4019(18)	3.628(1)
	3.669(9)	3.650(4)	3.558(2)	3.293(13)	3.4346(19)	3.133(1)
				3.657(4)	3.454(2)	
Cluster "radius"	6.198(4)	6.285(2)	6.175(1)	6.214(1)	6.410(2)	5.974(1)

at distance 3.38-3.5 Å, forming a somewhat distorted pyramid. The μ_2-S atoms are located inside a distorted octahedron, formed by Sn, Cd and four Cs atoms (see Figure 4b).

There is some analogy between the $[M_4Sn_4S_{17}]^{10-}$ clusters and the adamantine clusters, e.g. $[Ge_4S_{10}]^{4-}$, in the sense that both posses tetrahedral T_d symmetry. They represent however different structural motifs that do not derive from one another. The $[M_4M'_4S_{17}]^{10-}$ is constructed from 6-membered rings having only the *boat* conformation whereas the adamantane homologues contain rings in the *chair* conformation. Interestingly, organic and oxide analogs for this cluster have been known for some time and have the stoichiometry $Si_8C_{17}H_{36}$ and $Na_{10}Be_4Si_4O_{17}$ respectively [25, 26]. The space group of $Na_{10}Be_4Si_4O_{17}$ is P-43m which is also the space group of compounds **II-IV** and **VI**. Selected bond distances and angles of all compounds are given in Table 8.

UV-vis-NIR spectroscopy

Electronic absorption spectroscopy in the range of 0.5-6 eV revealed sharp optical absorptions for all six compounds, Figure 5a-c. Since the optically active species are molecular complexes, these transitions are between "localized" energy levels. They can be assigned to S→M charge transfer transitions across a higher occupied to a lowest unoccupied molecular orbital gap (HOMO-LUMO gap).

$K_{10}Zn_4Sn_4S_{17}$ has a sharp transition beginning at 3.2 eV (387.5 nm), whereas for $K_{10}Zn_4Ge_4S_{17}$ the absorption begins approximately at 3.34 eV. For $K_{10}Mn_4Sn_4S_{17}$, $K_{10}Fe_4Sn_4S_{17}$ $K_{10}Co_4Sn_4S_{17}$, and $Cs_{10}Cd_4Sn_4S_{17}$ the optical absorptions were observed at 2.25, 1.75, 1.31, and 3.16 eV respectively. The Co and Fe analogs also have weak spectral features below these absorption edges and they are attributed to d-d transitions within the transition metal.

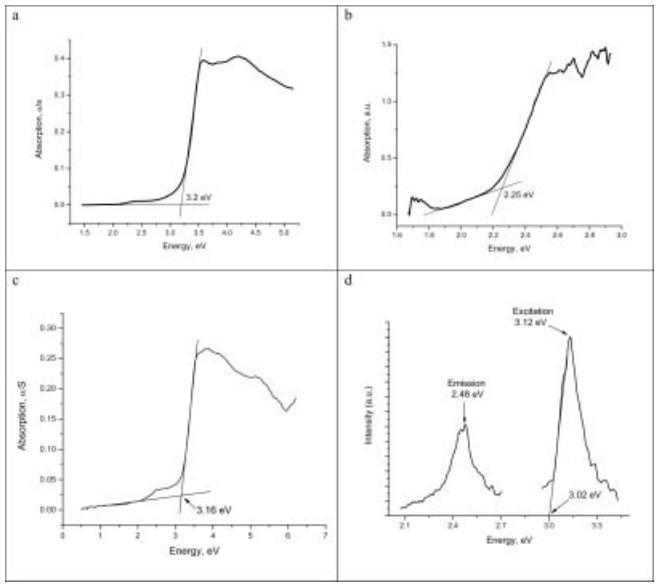

Figure 5 (a) Electronic absorption UV-VIS-NIR spectra of polycrystalline $K_{10}Zn_4Sn_4S_{17}$, (b) single-crystal visible absorption spectrum of $K_{10}Mn_4Sn_4S_{17}$, (c) spectrum of polycrystalline $Cs_{10}Cd_4Sn_4S_{17}$, (d) Photoluminescence and excitation spectra of polycrystalline $Cs_{10}Cd_4Sn_4s_{17}$ at 77 K.

Luminescence

Of all compounds examined only $Cs_{10}Cd_4Sn_4S_{17}$ (**V**) and $K_{10}Zn_4Ge_4S_{17}$ (**VI**) showed weak luminescence properties when excited above their absorption edge, see Figure 5d, 6a-b. $Cs_{10}Cd_4Sn_4S_{17}$ has weak yellow emission at room temperature, but at 77 K the luminescence becomes much stronger. With an exciting line of 3.12 eV (397 nm) we observed intense emission at 2.48 eV (501 nm), see Figure 5d. The extrapolation of the excitation band to zero intensity, gives a band-gap of 3.02 eV which agrees with the value of 3.16 eV obtained using diffuse-reflectance measurements.

Using the cathodoluminescence technique a very broad asymmetric emission spectrum was observed for compound **V** which could be deconvoluted using Gaussian functions into three emission peaks: the major peak occurs at 2.9 eV (423 nm) and two relatively small peaks at 2.6 eV (477 nm) and at 2.4 eV (509 nm), see Figure 6a. The existence of multiple signals is indicative of a defect origin of the emission property of this compound.

The room temperature cathodoluminescence spectrum of compound **VI** showed only a single maximum at 2.15 eV (578 nm), see Figure 6b. Given the wide gap of 3.34 eV for this compound the emission energy lies in the mid-gap region and suggests that it originates from a defect rather than from a HOMO-LUMO electron-hole recombination.

Luminescence has been observed in several open-framework supertetrahedral chalcogenide compounds and it was established that proper variation of the composition could result in inorganic-organic phosphors with tunable emission properties [6]. In addition, in the mesostructured cetylpyridinium-M-Ge_4S_{10} system the luminescent properties of the surfactant molecules could be altered by the presence of the non-emitting M-Ge_4S_{10} part [27]. Perhaps we may expect that mesostructured systems with fluorescent inorganic components (e.g. $[Cd_4Sn_4S_{17}]^{10-}$) and fluorescent organic surfactant could exhibit interesting luminescent hybrid materials.

Solid State NMR measurements

The ^{119}Sn MAS NMR spectrum of $Cs_{10}Cd_4Sn_4S_{17}$ (**V**) is shown in Figure 7. The ^{119}Sn chemical shift of 49.9 ppm is within the range (−25 to +70 ppm) typically observed for tetrahedrally coordinated tin sulfides [28, 29, 30]. The T_1 value was ∼ 300 s and the best-fit chemical shift anisotropy principal values were δ_{11}, δ_{22}, δ_{33} = 91, 58, 0 ppm with an uncertainty of ± 10 ppm in each value. The value of $\delta_{11} - \delta_{33}$ (∼ 90 ppm) is consistent with a tetrahedrally coordi-

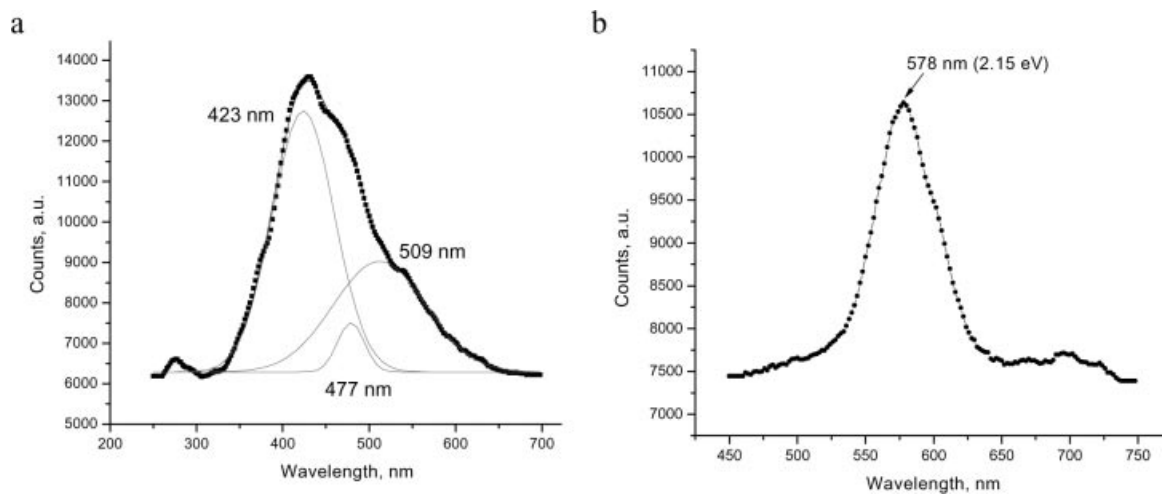

Figure 6 (a) Cathodoluminescence spectrum of $Cs_{10}Cd_4Sn_4S_{17}$. The plots indicates the three different contributions determined from Gaussian line shape analysis. (b) cathodoluminescence spectrum of $K_{10}Zn_4Ge_4S_{17}$.

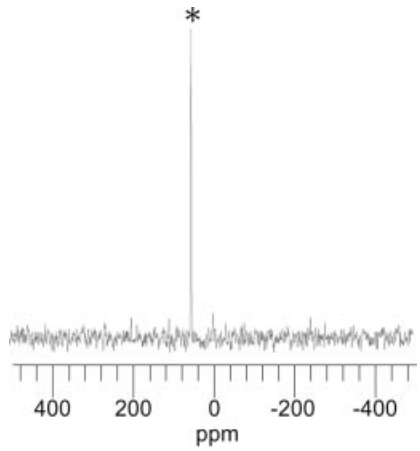

Figure 7 Magic angle solid-state ^{119}Sn NMR spectrum of $Cs_{10}Cd_4Sn_4S_{17}$ with a single isotropic peak at 49.9 ppm.

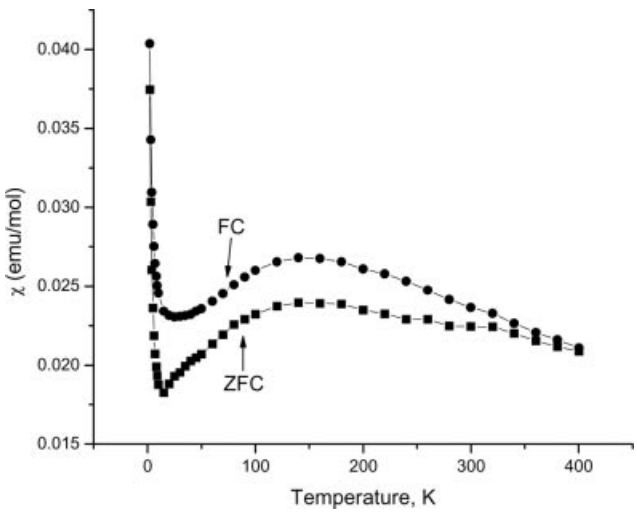

Figure 8 The molar magnetic susceptibility of $K_{10}Fe_4Sn_4S_{17}$ (**IV**) from 2 to 400 K. The applied field was 100 Oe. Evident is the strong divergence in the susceptibility between zero field cooled and field cooled data begins at around 400 K.

nated Sn^{4+} and with the high overall symmetry observed in the single crystal structure of this compound. The ^{119}Sn MAS NMR spectrum of **I** (not shown here) was similar with a CS of 49.2 ppm and a ~ 150 ppm value of $\delta_{11} - \delta_{33}$.These parameters are also consistent with the highly symmetric tetrahedral environment of tin in this compound.

Magnetic properties

The magnetic susceptibility of $K_{10}Fe_4Sn_4S_{17}$ and $K_{10}Mn_4Sn_4S_{17}$ over a wide range of temperature is shown in Figure 8 and 9. The Curie-Weiss law is not followed at any temperature interval. Instead a broad maximum is observed in the susceptibility curve at ~140 K and 90 K respectively. The maxima are attributed to antiferromagnetic interactions between the spins on the Fe^{2+} atoms (d^6) and Mn^{2+} (d^5) and in the $[M_4S]^{6+}$ core of the cluster. The Mn-Mn and Fe-Fe distances in this core are 3.873(1) Å and 3.788(1) Å respectively (see Table 8).

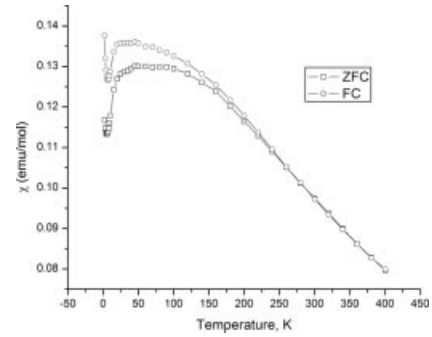

Figure 9 The molar magnetic susceptibility of $K_{10}Mn_4Sn_4S_{17}$ (**II**) from 2 to 400 K. The divergence in the susceptibility between zero field cooled and field cooled data begins at around 290 K, 240 K and 200 K for applied field of 100 Oe, 500 Oe and 1000 Oe respectively. With increasing applied field, there is a reduction of the divergence in the susceptibility between the zero field cooled and field cooled data.

A rather peculiar property of the magnetic susceptibility of both $K_{10}Fe_4Sn_4S_{17}$ and $K_{10}Mn_4Sn_4S_{17}$ is the noticeable difference between the zero field cooled (ZFC) and field cooled (FC) curves. This discrepancy with field diminishes with increasing field strength and it nearly disappears above 1000 Oe. At this stage we do not understand the origin of this behavior and we speculate that it might be associated with possible spin-glass phenomena. The probable cause for spin glass behavior in general is disorder and magnetic frustration [31, 32]. In $K_{10}Mn_4Sn_4S_{17}$ disorder and frustration might arise from random cluster rotations in the structure. The observed high thermal parameters of the terminal sulfide ligands of the cluster and alkali atoms as well as the partial occupancy of potassium ions may be consistent with these effects.

The results are comparable also for **III** and **IV.** For that reason only qualitative discussion of the magnetic properties of **II** are presented here, and more quantitative results for all three compounds will be published elsewhere. More work on the magnetism of the transition metal $[M_4M'_4S_{17}]^{10-}$ clusters is necessary to further understand this behavior.

Concluding Remarks

$K_{10}M_4Sn_4S_{17}$ (M = Mn, Fe, Co, Zn), $Cs_{10}Cd_4Sn_4S_{17}$ and $K_{10}Zn_4Ge_4S_{17}$ are examples of what probably is a considerable group of analogs with the basic structural supertetrahedral $[M_4M'_4S_{17}]^{10-}$ unit. The successful synthesis of the germanium analog $K_{10}Zn_4Ge_4S_{17}$ and the existence of Se analogs indicate that the $[M_4M'_4S_{17}]^{10-}$ cluster is very adaptable to extensive substitution. Preliminary synthetic experiments using selenium based polychalcogenide fluxes also resulted in the preparation of inorganic $[M_4M'_4Se_{17}]^{10-}$ molecular cluster (will be published elsewhere). As a consequence of the presence of two kinds of metal centers in the cluster (M and M′), these compounds could simultaneously possess unusual magnetic and per-

haps optical properties. The fact that compounds **I-VI** are soluble in water and organic solvents, surviving even for a limited time, makes them attractive as potential precursors for a variety of mesostructured materials. Finally, the magnetic properties of the Mn, Fe and Co compounds are unusual and call for further studies.

Acknowledgment. Financial support from the National Science Foundation (DMR-0127644 and CHE-0211029 Chemistry Research Group) is gratefully acknowledged. The authors thank Dr. R. Loloee for assistance in magnetic measurements and E. Danielewicz for assistance in cathodoluminescence measurements.

References

[1] M. J. MacLachlan, N. Coombs, G. A. Ozin, *Nature (London)* **1999**, *397*, 681; K. K. Rangan, S. J. L. Billinge, V. Petkov, J. Heising, M. G. Kanatzidis, *Chem. Mater.* **1999**, *11*, 2629.
[2] P. N. Trikalitis, K. K. Rangan, T. Bakas, M. G. Kanatzidis, *Nature (London)* **2001**, *410*, 671; P. N. Trikalitis, K. K. Rangan, M. G. Kanatzidis, *J. Am. Chem. Soc.* **2002**, *124*, 2604; P. N. Trikalitis, K. K. Rangan,; T. Bakas, M. G. Kanatzidis, *J. Am. Chem. Soc.* **2002**, *124*, 12255; A. E. Riley, S. H. Tolbert, *J. Am. Chem. Soc.* **2003**, *125*, 4551.
[3] G. Ferey, *Angew. Chem.* **2003**, *115*, 2680; *Angew. Chem. Int. Ed.* **2003**, *42*, 2576.
[4] H. L. Li, J. Kim, M. O'Keeffe, O. M. Yaghi, *Angew. Chem. Int. Ed.* **2003**, *42*, 1819.
[5] C. L. Cahill, J. B. Parise, *J. Chem. Soc., Dalton Trans.* **2000**, *9*, 1475.
[6] H. L. Li, A. Laine, M. O'Keeffe, O. M. Yaghi, *Science* **1999**, *283*, 1145.
[7] H. L. Li, J. Kim, T. L. Groy, M. O'Keeffe, O. M. Yaghi, *J. Am. Chem. Soc.* **2001**, *123*, 4867.
[8] C. Wang, Y. Q. Li, X. H. Bu, N. F. Zheng, O. Zivkovic, C. S. Yang, P. Y. Feng, *J. Am. Chem. Soc.* **2001**, *123*, 11506.
[9] W. P. Su, X. Y. Huang, J. Li, H. X. Fu, *J. Am. Chem. Soc.* **2002**, *124*, 12944.
[10] X. H. Bu, N. F. Zheng, Y. Q. Li, P. Y. Feng, *J. Am. Chem. Soc.* **2002**, *124*, 12646.
[11] O. Palchik, R. G. Iyer, J. H. Liao, M. G. Kanatzidis, *Inorg. Chem.* **2003**, *42*, 5052.
[12] M. G. Kanatzidis, J. H. Liao, G. A. Marking, US Patent 5, 614, 128, **1997**.
[13] S. Dehnen, M. K. Brandmayer, *J. Am. Chem. Soc.* **2003**, *125*, 6618.
[14] C. Zimmermann, M. Melullis, S. Dehnen, *Angew. Chem.* **2002**, *114*, 4444; *Angew. Chem. Int. Ed.* **2002**, *41*, 4269.
[15] J. H. Liao, C. Varotsis, M. G. Kanatzidis, *Inorg. Chem.* **1993**, *32*, 2453.
[16] G. D. Albertelli, J. A. Cowen, C. N. Hoff, T. A. Kaplan, S. D. Mahanti, J. H. Liao, M. G. Kanatzidis, *Phys. Rev. B* **1997**, *55*, 11056.
[17] J. A. Aitken, G. A. Marking, M. Evain, L. Iordanidis, M. G. Kanatzidis, *J. Solid State Chem.* **2000**, *153*, 158; G. Kortüm, *Reflectance spectroscopy. Principles, methods, applications*; Springer: Berlin, Heidelberg, New York, 1969.
[18] Siemens Analytical X-Ray Instruments Inc., 1995.
[19] SHELXTL V-5; Siemens Analytical X-Ray Instruments Inc.: Madison, WI
[20] A. L. J. Spek, *Appl. Crystallogr.* **2003**, *36*, 7.
[21] K. Chondroudis, M. G. Kanatzidis, *Inorg. Chem.* **1995**, *34*, 5401.
[22] T. B. Massalski, H. Okamoto, *Binary alloy phase diagrams*; 2nd ed.; ASM International: Materials Park, Ohio, 1990.
[23] O. Palchik, M. G. Kanatzidis, unpublished results.
[24] H. O. Stephan, M. G. Kanatzidis, G. Henkel, *Angew. Chem. Int. Ed. Engl.* **1996**, *35*, 2135.
[25] H. G. von Schnering, G. Sawitzki, K. Peters, K. F. Z. Tebbe, *Z. Anorg. Allg. Chem.* **1974**, *404*, 38.
[26] L. Eriksson, S. Frostang, J. Grins, *Acta Crystallogr.* **1990**, *B46*, 736.
[27] K. K. Rangan, P. N. Trikalitis, M. G. Kanatzidis, *J. Am. Chem. Soc.* **2000**, *122*, 10230.
[28] K. K. Rangan, P. N. Trikalitis, C. Canlas, T. Bakas, D. P. Weliky, M. G. Kanatzidis, *Nano Lett.* **2002**, *2*, 513.
[29] T. Jiang, G. A. Ozin, R. L. Bedard, *Adv. Mater.* **1994**, *6*, 860.
[30] J. Mason, *Multinuclear NMR*; Plenum Press: New York, 1987.
[31] J. A. Mydosh, *Spin glasses: an experimental introduction*; Taylor & Francis: London; Washington, DC, 1993.
[32] G. Toulouse, *Commun. Phys. (London)* **1977**, *2*, 115.

